BROADBAND STUDY WITH *SUZAKU* OF THE MAGNETAR CLASS

T. ENOTO[1,6], K. NAKAZAWA[1], K. MAKISHIMA[1,2], N. REA[3], K. HURLEY[4], AND S. SHIBATA[5]

[1] Department of Physics, University of Tokyo, 7-3-1 Hongo, Bunkyo-ku, Tokyo 113-0033, Japan; enoto@ceres.phys.s.u-tokyo.ac.jp, enoto@stanford.edu
[2] High Energy Astrophysics Laboratory, Institute of Physical and Chemical Research (RIKEN), Wako, Saitama 351-0198, Japan
[3] Institut de Ciencies de l'Espai (ICE-CSIC, IEEC), Campus UAB, Facultat de Ciencies, Torre C5-parell, 2a planta, 08193 Bellaterra (Barcelona), Spain
[4] Space Sciences Laboratory, 7 Gauss Way, University of California, Berkeley, CA 94720-7450, USA
[5] Department of Physics, Yamagata University, Yamagata 990, Japan

ABSTRACT

Broadband (0.8–70 keV) spectra of the persistent X-ray emission from nine magnetars were obtained with *Suzaku*, including three objects in apparent outburst. The soft X-ray component was detected from all of them, with a typical blackbody temperature of $kT \sim 0.5$ keV, while the hard-tail component, dominating above $\sim$10 keV, was detected at $\sim$1 mCrab intensity from seven of them. Therefore, the spectrum composed of a soft emission and a hard-tail component may be considered to be a common property of magnetars, both in their active and quiescent states. Wideband spectral analyses revealed that the hard-tail component has a 1–60 keV flux, F_h, comparable to or even higher than that carried by the 1–60 keV soft component, F_s. The hardness ratio (HR) of these objects, defined as $\xi \equiv F_h/F_s$, was found to be tightly anti-correlated with their characteristic age τ_c as $\xi = (3.3 \pm 0.3) \times (\tau_c/1 \text{ kyr})^{-0.67 \pm 0.04}$ with a correlation coefficient of -0.989, over the range from $\xi \sim 10$ to $\xi \sim 0.1$. Magnetars in outburst states were found to lie on the same correlation as relatively quiescent ones. This HR is also positively correlated with their surface magnetic fields with a correlation coefficient of 0.873. In addition, the hard-tail component becomes harder toward sources with older characteristic ages, with the photon index changing from $\sim$1.7 to $\sim$0.4.

Key words: stars: evolution – stars: magnetars – stars: magnetic field – stars: neutron

1. INTRODUCTION

Soft gamma repeaters (SGRs) and anomalous X-ray pulsars (AXPs) are considered to form a distinct class of neutron stars, collectively called "magnetars," and are thought to have magnetic fields exceeding the critical value of $B_{QED} = 4.4 \times 10^{13}$ G (Thompson & Duncan 1995, 1996; for a recent review see, e.g., Mereghetti 2008; Woods & Thompson 2006). Although their radiation, mainly emerging in the X-ray frequency, is considered to be powered by their huge magnetic energies, little is known about how the postulated strong magnetic fields are dissipated and converted into the radiation. It is hence imperative at this stage to examine their emission properties for any empirical relations that provide a more unified characterization of these enigmatic objects.

Through hard X-ray imaging observations with *INTEGRAL*, some persistently bright magnetars were discovered to emit not only the well-known soft component (with a temperature of $kT \sim 0.5$ keV), but also a distinct hard-tail component which emerges above $\sim$10 keV with an extremely hard photon index of $\Gamma_h \simeq 1$ (e.g., Kuiper et al. 2006; Götz et al. 2006). The hard-tail component has also been detected from transient magnetars in outburst states, including SGR 0501+4516 (Rea et al. 2009; Enoto et al. 2010b) and 1E 1547.0−5408 (Enoto et al. 2010a). This unusual new component, though not yet observed from all magnetars, is expected to provide a clue to the emission process and the magnetic dissipation mechanism in magnetars.

To perform wide-band spectroscopy of magnetars covering these two components, multi-satellite observations have generally been employed. However, the hard-tail intensity ($\lesssim$10 mCrab) of these objects requires much longer exposures than are usually spent in observing their soft components. As a

result, it has so far been difficult to obtain strictly simultaneous wide-band spectra of these sources which are more or less time variable. In the present Letter, we report on *Suzaku* (Mitsuda et al. 2007) observations of most of the presently known magnetars, studying for the first time soft and hard X-ray spectra taken simultaneously. We thus found a strong correlation between magnetars' hardness ratio (HR) and characteristic ages.

2. OBSERVATION AND ANALYSIS

Since its launch, *Suzaku* has performed 15 pointed observations of 10 magnetars, including 5 targets in a *Suzaku* Key Project in 2009. We analyzed all these *Suzaku* data in a unified way, except for 1E 1048.1−5937, for which the data are not yet public as of 2009 November. This included re-analyses of the data from previously reported observations; i.e., SGR 1806−20 (Esposito et al. 2007; Nakagawa et al. 2009), SGR 1900+14 (Nakagawa et al. 2009), 1E 1841−045 (Morii et al. 2008), CXOU J164710.2−455216 (Naik et al. 2008), SGR 0501+4516 (Enoto et al. 2009, 2010b), and 1E 1547.0−5408 (Enoto et al. 2010a). Table 1 summarizes the observations utilized in the present Letter. Among them, three sources, namely, CXOU J164710.2−455216, SGR 0501+4516, and 1E 1547.0−5408, were observed during bursting periods. Our sample, though not complete, covers 9 sources out of the $\sim$15 magnetars known to date.

From each observation, we extracted events for persistent X-ray emission using the X-ray Imaging Spectrometer (XIS; Koyama et al. 2007) and the Hard X-ray Detector (HXD; Takahashi et al. 2007), which cover energy ranges of 0.2–12 keV and 10–600 keV, respectively. The XIS and HXD data were processed with the pipeline processing version 2.0 or later, and events were discarded if they were acquired in the South Atlantic Anomaly or in regions of low cutoff rigidity ($<$6 GV for the XIS and $<$8 GV for the HXD), or at low Earth elevation

Table 1
Log of *Suzaku* Observations of Magnetars

Name[a]	P[b] (s)	$\dot{P}$[b] 10^{-11} (s s^{-1})	B_s[c] 10^{14} (G)	τ_c[d] (kyr)	ObsID	Date (yy-mm-dd)	Exp.[e] (ks)	Model[f] (χ^2/dof)	Abs. F_x[g] F_{15-60}/F_{2-10} $15-60/2-10$	Unabs. F_x[h] F_h/F_s $1-60/1-60$	HR[i] $\xi=F_h/F_s$	Γ_h[j]
								Soft gamma-ray repeater				
1806−20	7.556	54.9	21	0.22	401092010	06-09-09	55.4	A(468.9/434)	30.2(3)/12.6(1)	$55.6^{+3.1}_{-2.3}/6.1^{+1.3}_{-0.9}$	$9.1^{+2.1}_{-1.3}$	1.7(1)
...	...	...	...	...	401021010	07-03-30	16.5	A(185.1/182)	46(10)/9.7(3)	$57.1^{+6.5}_{-6.0}/6.8^{+1.1}_{-0.8}$	$8.4^{+1.7}_{-1.3}$	1.2(1)
...	...	...	...	...	402094010	07-10-14	50.1	A(239.3/240)	24(3)/8.6(2)	$38.6^{+4.0}_{-7.7}/4.7^{+1.0}_{-0.7}$	$8.2^{+2.0}_{-1.3}$	1.6(2)
1900+14	5.169	7.78	6.4	1.1	401022010	06-04-01	14.4	A(145.5/156)	15(6)/4.5(3)	$18.7^{+4.0}_{-7.7}/4.3^{+0.3}_{-0.2}$	$4.4^{+1.0}_{-1.8}$	1.2(5)
...	...	...	...	...	404077010	09-04-26	42.1	A(433.6/393)	8(4)/3.2(2)	$10.7^{+2.4}_{-2.1}/4.3\pm0.2$	$2.5^{+0.6}_{-0.5}$	1.4(3)
0501+45	5.762	0.5	1.7	18	903002010	08-08-26	33.5	C(151.2/149)	27(6)/27.2(5)	$27.4^{+6.9}_{-6.3}/47.5^{+1.0}_{-1.4}$	$0.58^{+0.15}_{-0.13}$	0.7(3)
					404078010	09-08-17	43.0	B(191.7/154)	<24/1.4(4)	<25/3.8 ± 0.2	<6.7	...
								Anomalous X-ray pulsars				
1547−54	2.070	2.32	2.2	1.4	903006010	09-01-28	33.5	A(298.9/278)	105(7)/57(1)	$159\pm5/56^{+1}_{-2}$	2.8 ± 0.1	1.54(5)
1841−04	11.775	4.16	7.1	4.5	401100010	06-04-19	63.5	B(462.9/262)	45(4)/26(2)	$49.7^{+1.6}_{-1.1}/34.4^{+0.5}_{-0.3}$	$1.44^{+0.05}_{-0.04}$	1.00(3)
1708−40	10.999	1.94	4.7	9.0	404080010	09-08-23	60.9	B(94.6/98)	27(6)/28.8(6)	$30.0^{+5.1}_{-4.2}/62.7^{+2.7}_{-3.0}$	$0.48^{+0.08}_{-0.07}$	1.1(3)
0142+61	8.688	0.20	1.3	70	402013010	07-08-13	101.6	B(434.4/408)	36(3)/64.4(2)	$36.3^{+7.1}_{-7.0}/181.1^{+0.5}_{-1.2}$	0.20 ± 0.04	0.3(1)
...	...	...	...	...	404079010	09-08-12	107.4	B(310.6/301)	30(4)/61.4(3)	$27.8^{+6.4}_{-6.3}/175.2^{+1.0}_{-1.2}$	0.16 ± 0.04	0.4(2)
1647−45	10.611	0.24	1.6	70	901002010	06-09-23	35.1	B(333.2/294)	··· /23.4(3)	··· /45.1 ± 0.5	··· -	··· -
2259+58	6.979	0.05	0.59	230	404076010	09-05-25	103.4	B(222.1/213)	<8.7/15.8(1)	<9.2/45.7 ± 0.4	<0.2	··· -

Notes.
[a] Abbreviated names represent SGR 1900+14, SGR 1806−20, SGR 0501+4516, 1E 1547.0−5408, 1E 2259+586, 4U 0142+61, CXO J164710.2−455216, 1RXS J170849.0−400910, and 1E 1841−045.
[b] P and $\dot{P}$ values are from the McGill SGR/AXP Online Catalog (http://www.physics.mcgill.ca/~pulsar/magnetar/main.html).
[c] Surface magnetic field strength estimated as $B_s = 3.2 \times 10^{19}(P\dot{P})^{1/2}$ G.
[d] Characteristic ages estimated as $\tau_c = P/2\dot{P}$ s.
[e] Effective exposures of the HXD.
[f] Model A: a blackbody plus a power-law model (BB+PL); Model B: a Comptonized blackbody plus the power law (CBB+PL); Model C: a blackbody and the Comptonized blackbody plus the power law (BB+CBB+PL).
[g] Absorbed X-ray fluxes (10^{-12} erg s^{-1} cm^{-2}) in the 15–60 keV and 2–10 keV bands. Quoted errors are statistical—only at the 90% confidence level.
[h] Unabsorbed X-ray fluxes (10^{-12} erg s^{-1} cm^{-2}) of the 1–60 keV soft component and the 1–60 keV hard-tail component. Statistical errors (1σ) are included. Systematic errors (1σ) are also included in the hard-tail component, calculated from the uncertainties in the PIN-NXB and in the cross normalization between the XIS and HXD-PIN.
[i] HR ξ, calculated from the two unabsorbed fluxes. Quoted errors are statistical and systematic 1σ level.
[j] Photon index of the hard-tail component. Quoted errors are statistical and systematic 1σ level. If the upper and lower errors are different, average errors are shown.

angles.[7] In addition, a fair number of short bursts, detected from SGR 0501+4516, 1E 1547.0−5408, and SGR 1806−20, were removed by discarding the XIS and HXD events which were detected within a time interval of a few seconds around each of these bursts (e.g., Enoto et al. 2010a). Studies of these burst events are beyond the scope of this Letter.

To create 0.8–10 keV XIS spectra, we accumulated the screened data from a source region typically within a 2′.0 radius of the target centroid and derived a background spectrum from adjacent regions on the same CCD chip. Since the background count rates are typically ~5% of the source rates, systematic uncertainties of the XIS background are negligible. Thanks to the use of appropriate window options, all the observations were free from XIS event pileup.

For each observation, an HXD-PIN spectrum was produced in the 10–70 keV range, after subtracting non-X-ray background (NXB) and cosmic X-ray background (CXB; typically ~4% of the NXB). We utilized NXB events which are simulated by the "tuned" model of Fukazawa et al. (2009) and the analytic CXB model by Moretti et al. (2009). In the case of sources near the Galactic center (i.e., SGR 1806−20 and

1RXS J170849.0−400910), we further subtracted Galactic ridge X-ray emission (GRXE; Krivonos et al. 2007; typically ≲3% level of the NXB), with a photon index fixed at 2.1 (Valinia & Marshall 1998) and normalizations specified by observations of nearby blank skies at similar Galactic latitudes. Systematic errors in these HXD-PIN spectra are dominated by reproducibility of the NXB model, which is typically ≲2% (1σ) (Fukazawa et al. 2009), while those of the CXB and GRXE are negligible. This effect is taken into account by changing the PIN-NXB within ±2%. The HXD-PIN field of view was clear of significant contaminating sources in these observations, except for the case of CXOU J164710.2−455216 (Naik et al. 2008), which was confused with GX 340+0. Source confusion was not an issue for the other eight sources, and we hence analyze these eight sources below.

3. RESULTS

Figure 1 shows background-subtracted and pulse-phase-averaged persistent spectra of the eight magnetars. The soft component was clearly observed from all of them, while the hard-tail component was successfully detected from seven of them at a typical intensity of ~1 mCrab (at ~30 keV). Assuming $\Gamma_h \sim 1$, any hard-tail flux from 1E 2259+586 was constrained to be less than 8.7×10^{-12} erg s^{-1} cm^{-2} in the

---
[7] Detailed criteria are listed at heasarc.nasa.gov/docs/suzaku/processing/criteria_hxd.html and heasarc.nasa.gov/docs/suzaku/processing/criteria_xis.html.
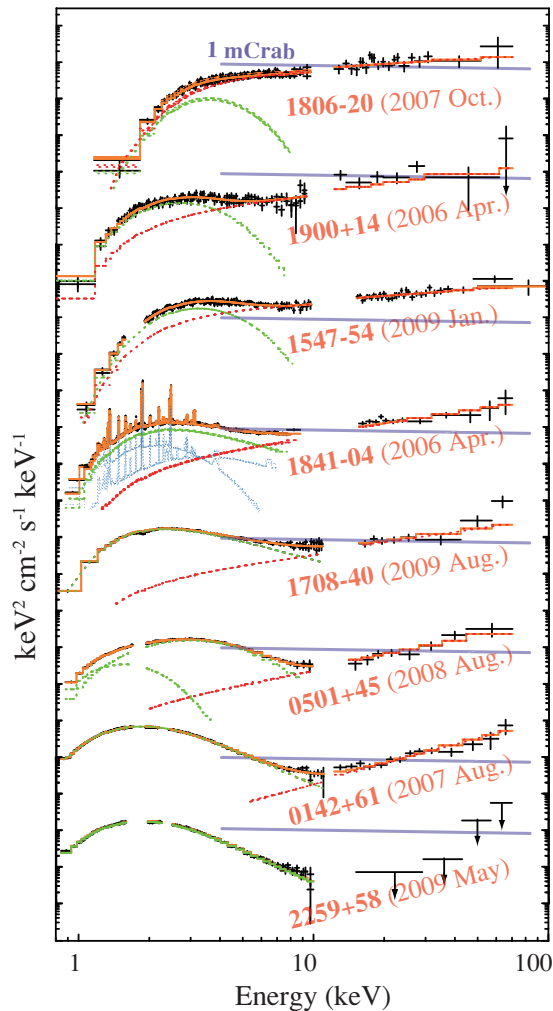
Figure 1. Background-subtracted νF_ν spectra of the persistent emission of the magnetars, shown after eliminating the instrumental responses. Interstellar absorption is included. Individual spectra are shown with offsets and are arranged in order of increasing characteristic age from top (young) to bottom (old). Blue horizontal lines indicate a 1 mCrab intensity. Green, red, and blue lines represent the soft component, the hard-tail component, and the SNR contamination (including line emission) in the 1E 1841−045 spectrum, respectively. If a source was observed more than once, one observation is shown. The GSO data of 1E 1547.0−5408 are included after Enoto et al. (2010a). The full names of the sources, which are shown here as abbreviations, are listed in a footnote to Table 1.

15–60 keV range, which is consistent with the previous result from *INTEGRAL* (Figure 10 in Kuiper et al. 2006). These *Suzaku* spectra reconfirm the previous *INTEGRAL* detections of the hard-tail component from some persistent sources, including 4U 0142+61, 1RXS J170849.0−400910, 1E 1841−045, SGR 1806−20, and SGR 1900+14 (Mereghetti et al. 2005; Kuiper et al. 2006; Götz et al. 2006; den Hartog et al. 2007, 2008). The absorbed 2–10 keV and 15–60 keV X-ray fluxes are summarized in Table 1. Thus, the hard-band flux is comparable to, or sometimes even higher than, that in the softer band.

The unified presentation in Figure 1 yields an intriguing inference that the hard-tail component becomes weaker for older objects. To quantify this property, we simultaneously fitted the XIS and the HXD spectra of each object with a common spectral model. For the hard-tail component, we employed a single power law for all the sources. The soft component of younger magnetars was reproduced by a single blackbody (Model A), but older sources required some modification to this model
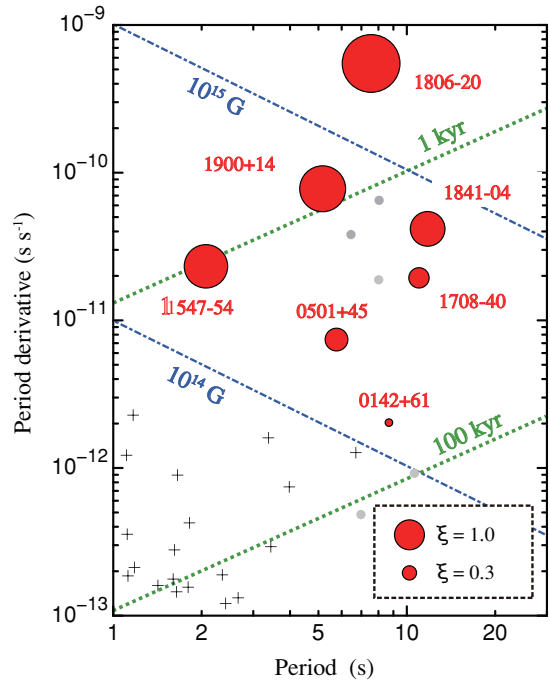

Figure 2. Portion of the P–$\dot{P}$ diagram of pulsars (Manchester et al. 2005; http://www.atnf.csiro.au/research/pulsar/psrcat/). Sizes of the red circles correspond to the ξ values in the present sample. Blue and green lines represent constant values of the magnetic field strength and the characteristic age, respectively. Small gray circles represent magnetars with upper limits on the hard-tail component, or those not observed with *Suzaku*. Ordinary radio pulsars are indicated by crosses.

due to a "soft-tail" excess around 8 keV, which is thought to arise via some sort of Comptonization process (Thompson et al. 2002; Lyutikov & Gavriil 2006; Rea et al. 2008). We therefore introduced an empirical Comptonized blackbody model (Model B; Tiengo et al. 2005; Halpern et al. 2008; Enoto et al. 2010a) and obtained successful fits in most cases. In the case of SGR 0501+4516, neither Model A nor B was acceptable, but a successful fit was obtained by adding a cooler blackbody to Model B (Model C; Enoto et al. 2010b). The XIS spectrum of 1E 1841−045 needed an additional plasma emission component from the surrounding supernova remnant.

From these fit results, we calculated absorption-corrected fluxes for the soft component F_s and the hard-tail component F_h, both defined in the 1–60 keV range. These values, given in Table 1, are considered physically more meaningful than the raw 2–10 keV and 15–60 keV fluxes, because the two components are separated, and the absorption is corrected. The lower boundary of 1 keV was adopted not only for F_s but also for F_h, because sources with young characteristic ages have substantial contributions of the hard-tail even in the lowest energy range at ∼0.8 keV (e.g., SGR 1806−20 in Figure 1). We may then define the "hardness ratio" (HR), $\xi \equiv F_h/F_s$. As shown in Table 1, the values of ξ range over almost 2 orders of magnitude from 0.2 to 10.

As visualized in Figure 2, ξ exhibits a clear gradient on the P–$\dot{P}$ plane. To assess this implication, we show in Figure 3 the values of ξ as a function of the characteristic age $\tau_c = P/2\dot{P}$ s and the surface magnetic field $B_s = 3.2 \times 10^{19}(P\dot{P})^{1/2}$ G, where the errors associated with ξ include both statistical and systematic errors. The latter is dominated by the 2% uncertainties of PIN-NXB (Section 2), with additional contributions (by ∼1% in ξ) from uncertainties in the XIS versus HXD cross
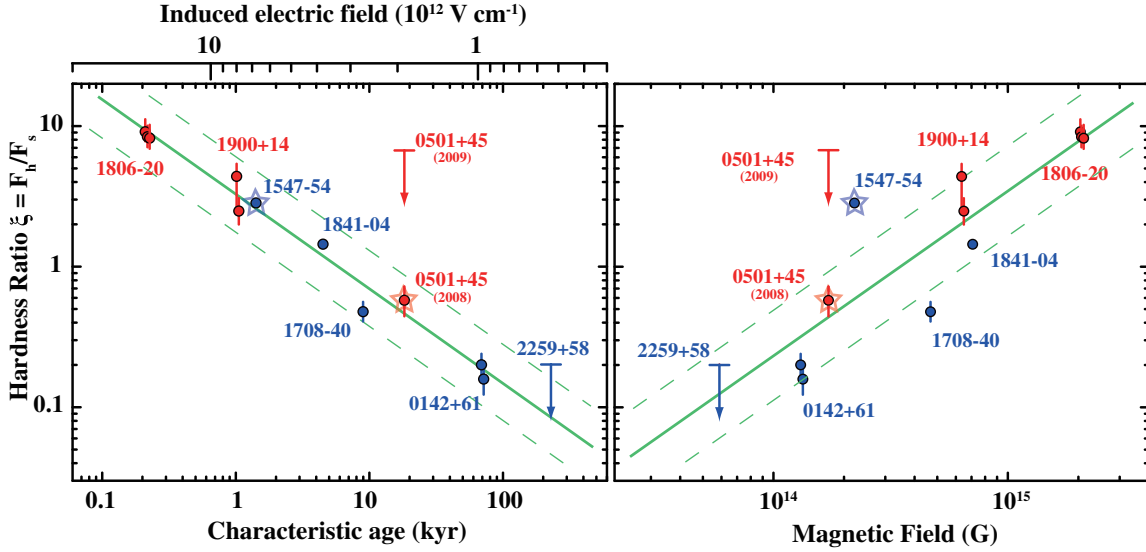
Figure 3. Left: correlation between the HR ξ and the characteristic age τ_c. Quoted errors are statistical plus systematic 1σ (Table 1). Upper limits are also shown for SGR 0501+4516 (second observation) and 1E 2259+586. Green solid and dashed lines represent the best fit of Equation (1) and their boundaries shifted by a factor of two, respectively. SGRs and AXPs are shown in red and blue, respectively, while burst-active sources are shown with star symbols. Right: same as the left panel, but plotted as a function of the surface magnetic field.

normalization. The figure indicates that ξ is indeed negatively (or positively) correlated with τ_c (or B_s).

After discarding the two upper limits in Figure 3, ξ is found to be correlated with τ_c and B_s with Pearson's linear cross-correlation coefficients of $r = -0.989$ and 0.873, respectively. Thus, ξ is very tightly correlated with τ_c, and to a lesser extent (as evident in Figure 2) with B_s. In order to evaluate the correlation in a non-parametric way, we further performed the Spearman's rank-order test, which gives correlation coefficients of $r_s = -0.963$ and 0.871 for τ_c and B_s, respectively, together with a chance probability in both cases of <0.001. Thus, these correlations are indeed significant. Fitting through the least squares method gave the best-fit linear correlation as

$$\xi = \frac{F_h}{F_s} = (3.3 \pm 0.3) \times \left(\frac{\tau_c}{1\ \mathrm{kyr}}\right)^{-0.67\pm0.04} \quad (1)$$

$$= (0.09 \pm 0.07) \times \left(\frac{B_s}{B_{\mathrm{QED}}}\right)^{1.2\pm0.2}, \quad (2)$$

with 1σ uncertainties. Since individual data points have rather small errors, we here added constant systematic errors to them, so as to make the fits acceptable with reduced chi-square values of $\sim$1. Around the ξ–τ_c linear fit, the data points scatter by no more than a factor of two in ξ.

Now that the ξ–τ_c and the ξ–B_s correlations were confirmed to be statistically significant, let us examine them for systematic effects. These correlations are unlikely to arise from some selection biases on the P–$\dot{P}$ plane, because these magnetars show a two-dimensional scatter in Figure 2 without any particular correlation between P and $\dot{P}$. These observations are also free from possible uncertainties due to independent variations of F_s and F_h, since in all sources these two quantities are based on strictly simultaneous measurements. In addition, multiple observations of the same objects at different epochs gave similar values of ξ (i.e., SGR 1806−20, SGR 1900+14, and 4U 0142+61 in Figure 3). Therefore, the essential features of Figure 2 are not considered to depend strongly on the epochs of observations.

Although the empirical Comptonized blackbody model (Model B) was employed in calculating F_s (and hence ξ) of 1RXS J170849.0−400910, SGR 0501+45, and 4U 0142+61, their values of ξ change only by a factor of 1.78, 1.09, and 0.94–1.09, respectively, if their soft component is modeled by two blackbodies that constitute another popular model. Thus, the implication of Figure 3 remains unchanged. The ξ–τ_c correlation also remains robust, even if we change the lower limit of the energy band from 1 keV to 0.5 keV. For example, this change reduces ξ by only 5% and 26% for the cases of SGR 1806−20 and 4U 0142+61, respectively. Similarly, if we raise the upper-limit energy of the hard-tail flux from 60 keV to 500 keV, the ξ–τ_c correlation also persists with $r = -0.788$ and $r_s = -0.825$. Therefore, the ξ–τ_c relation can be considered to represent a model-independent property of our sample of magnetars. Detailed spectral analyses of our sample objects will be described elsewhere, together with separate studies of pulsed and un-pulsed signals.

4. DISCUSSION AND CONCLUSION

Including most of the known SGRs and AXPs, the present data set provides the first simultaneous coverage of their soft and hard X-ray spectra (Figure 1). This has led to a discovery of the ξ–τ_c and ξ–B_s correlations in Figure 3. These tight correlations suggest that the values of ξ in the present objects approximately behave as a one parameter family (a single valued function) determined uniquely by P and $\dot{P}$. Among possible physical quantities expressed as simple combinations of P and $\dot{P}$, the characteristic age τ_c may be regarded as a likely determinant of ξ (see Figure 2). Then, by regarding τ_c as an indicator of the age in assuming a self-similar spin-down, and further noting that our sample covers a significant ($\sim$50%) fraction of the presently cataloged objects of these two classes, the ξ–τ_c correlation is considered to represent a common spectral evolution of them. Since both SGRs and AXPs follow the same correlations, the present result provides another support to the increasing evidence that these subsets are intrinsically considered the same kinds of object, namely, "magnetars."
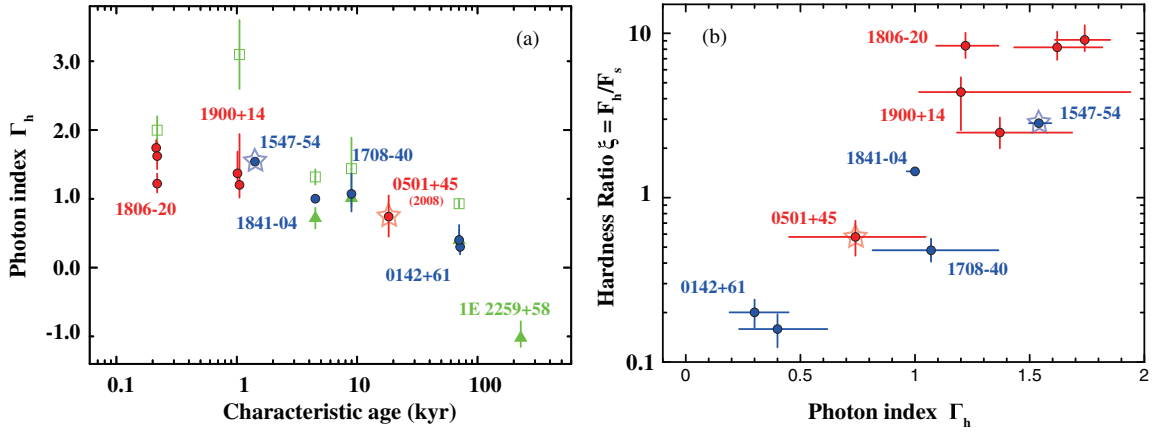
Figure 4. (a) Photon indices Γ_h of the hard-tail component of the present sample, plotted as a function of the characteristic age. Quoted errors are statistical and systematic 1σ. Colors and symbols are the same as in Figure 3. Green squares and triangles represent photon indexes of pulsed and total fluxes, respectively, after Kaspi & Boydstun (2010). (b) Relation between Γ_h and ξ.

From the burst-active magnetars SGR 0501+4516 and 1E 1547.0−5408, we successfully detected the hard-tail components. On the ξ−τ_c correlation, their ξ values generally agree with data points of the other magnetars, which mainly refer to quiescent or less active states. Therefore, the bursting activity of a magnetar is thought to cause a significant enhancement in the hard component, roughly to the same intensity as the soft component, which is known to increase by 1–2 orders of magnitude (Tam et al. 2008; Rea et al. 2009; Enoto et al. 2010a). The upper limit on the second observation of SGR 0501+4516 is consistent with this picture. These results further suggest that the basic mechanism of quiescent wide-band emission is retained during increased activity.

In addition to the above interpretation invoking τ_c, the same magnetar ξ−τ_c correlation may be interpreted in an alternative way. The strong magnetic field B, combined with the rotation, would induce an electric field up to

$$|\vec{E}| \sim R\Omega B$$

$$= 2.6 \times 10^{12} \frac{V}{cm} \left(\frac{6\ s}{P} \cdot \frac{\dot{P}}{10^{11}\ s\ s^{-1}} \right)^{1/2} \left(\frac{R}{10\ km} \right)$$

$$\propto \sqrt{\frac{1}{\tau_c}} \tag{3}$$

where R and Ω are the distance from the center of the star and the angular frequency, respectively. Thus, τ_c can be uniquely converted to $|\vec{E}|$, as shown at the top of Figure 3 (left). Thus, the magnetar ξ−τ_c correlation can also be regarded as a correlation between ξ and $|\vec{E}|$. If so, the hard-tail component, which should require the presence of particles more energetic than ∼100 keV, might be related to particle acceleration by this induced electric field.

A closer inspection of Figure 1 suggests a hardening of the hard-tail component for objects with larger τ_c. This is more clearly shown in Figure 4(a), where Γ_h is observed to evolve from ∼1.7 to ∼0.4. Such a correlation was first pointed out in the 1–10 keV band by Marsden & White (2001) and recently extended into hard X-rays by Kaspi & Boydstun (2010). The latter authors found a correlation of Γ_h with B_s or $\dot{P}$, with implications similar to those of our Figure 4(a). In contrast, they did not find any correlations that can be compared with our

Figure 3, presumably due to lack of simultaneity between the soft and hard X-ray measurements. Thanks to the simultaneous observations with *Suzaku*, we can plot, in Figure 4(b), the values of ξ as a function of Γ_h. Contrary to normal expectations that sources with lower broadband HRs should have softer (larger) values of Γ_h, this figure reveals an opposite correlation: that older magnetars with weaker hard-tail fluxes (smaller ξ) in fact have harder (smaller) slopes Γ_h. Since this is not affected by the selection of energy bands (Section 3), such a trend should imply an intrinsic property of the hard-tail production mechanism.

The present magnetar observations require the hard-tail emission mechanism to satisfy both the ξ−τ_c correlation and the hardening of the hard-tail component toward older objects. The difference of Γ_h among the sources rules out those models which predict a fixed common hard-tail slope (e.g., the fast-mode breakdown model; Heyl & Hernquist 2005). Such a large variation of Γ_h with τ_c is not expected by a thermal bremsstrahlung model from the transition layer on the stellar surface, either (Thompson & Beloborodov 2005; Beloborodov & Thompson 2007). Similarly, observed Γ_h values have not yet been reproduced by existing resonant magnetic Compton upscattering models (Baring & Harding 2007; Fernández & Thompson 2007). It remains to be examined whether the results of the present observations can be explained by any of the existing (or future) theoretical explanations (e.g., those based on the "twisted magnetosphere" model; Thompson et al. 2002).

As an alternative possibility, a photon-splitting process can act to produce the hard-tail emission. At the neutron star surface, sub-MeV photons can be produced through electron–positron annihilation or resonant magnetic Compton upscatterings. Since there is no low energy threshold for the photon splitting (Harding & Lai 2006), these sub-MeV photons may repeat splitting (Harding et al. 1997; Baring & Harding 2001) in the strong field, to form the hard continuum downward toward lower energies. In this case, the higher magnetic fields of younger magnetars will allow the photons to repeat splitting toward lower energies, thus making Γ_h larger in agreement with our figure.

REFERENCES

Baring, M. G., & Harding, A. K. 2001, ApJ, 547, 929
Baring, M. G., & Harding, A. K. 2007, Ap&SS, 308, 109
Beloborodov, A. M., & Thompson, C. 2007, Ap&SS, 308, 631
den Hartog, P. R., Kuiper, L., Hermsen, W., Kaspi, V. M., Dib, R., Knödlseder, J., & Gavriil, F. P. 2008, A&A, 489, 245
den Hartog, P. R., Kuiper, L., Hermsen, W., Rea, N., Durant, M., Stappers, B., Kaspi, V. M., & Dib, R. 2007, Ap&SS, 308, 647
Enoto, T., et al. 2009, ApJ, 693, L122
Enoto, T., et al. 2010a, PASJ, 62, 475
Enoto, T., et al. 2010b, ApJ, 715, 665
Esposito, P., et al. 2007, A&A, 476, 321
Fernández, R., & Thompson, C. 2007, ApJ, 660, 615
Fukazawa, Y., et al. 2009, PASJ, 61, 17
Götz, D., Mereghetti, S., Tiengo, A., & Esposito, P. 2006, A&A, 449, L31
Halpern, J. P., Gotthelf, E. V., Reynolds, J., Ransom, S. M., & Camilo, F. 2008, ApJ, 676, 1178
Harding, A. K., Baring, M. G., & Gonthier, P. L. 1997, ApJ, 476, 246
Harding, A. K., & Lai, D. 2006, Rep. Prog. Phys., 69, 2631
Heyl, J. S., & Hernquist, L. 2005, MNRAS, 362, 777
Kaspi, V. M., & Boydstun, K. 2010, ApJ, 710, L115
Koyama, K., et al. 2007, PASJ, 59, 23
Krivonos, R., Revnivtsev, M., Churazov, E., Sazonov, S., Grebenev, S., & Sunyaev, R. 2007, A&A, 463, 957
Kuiper, L., Hermsen, W., den Hartog, P. R., & Collmar, W. 2006, ApJ, 645, 556

Lyutikov, M., & Gavriil, F. P. 2006, MNRAS, 368, 690
Manchester, R. N., Hobbs, G. B., Teoh, A., & Hobbs, M. 2005, VizieR Online Data Catalog, 7245, 0
Marsden, D., & White, N. E. 2001, ApJ, 551, L155
Mereghetti, S. 2008, A&AR, 15, 225
Mereghetti, S., Götz, D., Mirabel, I. F., & Hurley, K. 2005, A&A, 433, L9
Mitsuda, K., et al. 2007, PASJ, 59, 1
Moretti, A., et al. 2009, A&A, 493, 501
Morii, M., et al. 2008, in AIP Conf. Ser. 983, 40 Years of Pulsars: Millisecond Pulsars, Magnetars and More, ed. C. Bassa et al. (Melville, NY: AIP), 268
Naik, S., et al 2008, PASJ, 60, 237
Nakagawa, Y. E., et al. 2009, PASJ, 61, 387
Rea, N., Zane, S., Turolla, R., Lyutikov, M., & Götz, D. 2008, ApJ, 686, 1245
Rea, N., et al. 2009, MNRAS, 396, 2419
Takahashi, T., et al. 2007, PASJ, 59, 35
Tam, C. R., Gavriil, F. P., Dib, R., Kaspi, V. M., Woods, P. M., & Bassa, C. 2008, ApJ, 677, 503
Thompson, C., & Beloborodov, A. M. 2005, ApJ, 634, 565
Thompson, C., & Duncan, R. C. 1995, MNRAS, 275, 255
Thompson, C., & Duncan, R. C. 1996, ApJ, 473, 322
Thompson, C., Lyutikov, M., & Kulkarni, S. R. 2002, ApJ, 574, 332
Tiengo, A., Mereghetti, S., Turolla, R., Zane, S., Rea, N., Stella, L., & Israel, G. L. 2005, A&A, 437, 997
Valinia, A., & Marshall, F. E. 1998, ApJ, 505, 134
Woods, P. M., & Thompson, C. 2006, in Compact stellar X-ray sources, ed. W. H. G. Lewin & M. van der Klis (Cambridge: Cambridge Univ. Press), 547